Journal of General Virology (2013), **94**, 1058–1068 **DOI** 10.1099/vir.0.048553-0

Cryo-electron microscopy reconstructions of triatoma virus particles: a clue to unravel genome delivery and capsid disassembly

J. Agirre,[1,2] G. Goret,[3] M. LeGoff,[3] R. Sánchez-Eugenia,[1] G. A. Marti,[4] J. Navaza,[3] D. M. A. Guérin[1,2] and E. Neumann[3]

Correspondence
E. Neumann
emmanuelle.neumann@ibs.fr
D .M. A. Guérin
diego.guerin@ehu.es

[1]Unidad de Biofisica (CSIC, UPV/EHU), PO Box 644, E-48080 Bilbao, Spain

[2]Fundación Biofísica Bizkaia, B° Sarriena S/N, 48940 Leioa, Bizkaia, Spain

[3]IBS, Institut de Biologie Structurale Jean-Pierre Ebel, UMR 5075 CNRS-CEA-UJF, 41 rue Jules Horowitz, F-38027 Grenoble, France

[4]Centro de Estudios Parasitológicos y de Vectores (CEPAVE-CCT-La Plata-CONICET-UNLP), 2#584 (1900) La Plata, Argentina

Received 2 October 2012
Accepted 27 December 2012

Triatoma virus (TrV) is a member of the insect virus family *Dicistroviridae* and consists of a small, non-enveloped capsid that encloses its positive-sense ssRNA genome. Using cryo-transmission electron microscopy and three-dimensional reconstruction techniques combined with fitting of the available crystallographic models, this study analysed the capsids corresponding to mature and several RNA-empty TrV particles. After genome release, the resulting reconstruction of the empty capsids displayed no prominent conformational changes with respect to the full virion capsid. The results showed that RNA delivery led to empty capsids with an apparent overall intact protein shell and suggested that, in a subsequent step, empty capsids disassemble into small symmetrical particles. Contrary to what is observed upon genome release in mammalian picornaviruses, the empty TrV capsid maintained a protein shell thickness and size identical to that in full virions.

INTRODUCTION

Triatoma virus (TrV), a positive-sense ssRNA virus with a small spherical non-enveloped capsid of ~300 Å in diameter (Muscio *et al.*, 1988; Czibener *et al.*, 2000), belongs to the genus *Cripavirus* (type species: cricket paralysis virus) within the family *Dicistroviridae* (Mayo, 2002). This virus infects several species of triatomines (Reduviidae: Hemiptera), the haematophagous insect vectors (kissing bugs) of Chagas disease (Pan American Health Organization, 2006). A solution of TrV purified using a sucrose gradient contains predominantly full virion particles (capsids containing the genome) and empty, RNA-free spherical particles (Estrozi *et al.*, 2008). A detailed analysis of full and empty TrV particles revealed that the TrV capsids of full particles are formed by four major viral proteins, VP1, VP2, VP3 and VP4, with respective molecular masses of 29.7, 28.4, 31.8 and 5.5 kDa, and a minor polypeptide, VP0, of 37.3 kDa. In contrast, the naturally produced empty capsids contain almost the same proteins as full particles (with the exception of VP4), but at least 30 % of their content corresponds to seven different polypeptides that result from misprocessing of the structural protein precursor P1. These peptides assemble into spherical particles that probably lose the capacity to enclose the genome (Agirre *et al.*, 2011). In addition, purified TrV also contains smaller symmetrical lip-shaped particles (LSPs; Estrozi *et al.*, 2008). So far, the origin of these small particles has not been identified, although it has been postulated that they are products of disassembled TrV capsids (Agirre *et al.*, 2011). Here, we demonstrated that TrV virions are stable under very acidic conditions. We also showed that a fresh sample of pure full TrV particles evolves, upon storage in neutral pH and under both standard ionic strength and temperature conditions, towards a solution composed of virions, empty particles (EPs) and LSPs. In addition, heating a sample of full virions to >50 °C induced RNA externalization and the formation of empty TrV capsids. This effect has been studied in detail for the picornaviruses poliovirus (PV; Bostina *et al.*, 2011) and human rhinovirus 2 (HRV2; Hewat *et al.*, 2002), and this experimental approach was considered a good model to emulate the structural changes that would permit the genome to exit the capsid. The crystallographic structure of the empty HRV2 capsid, which has been determined recently at 3.0 Å resolution (Garriga *et al.*, 2012), validated a previous cryo-transmission electron microscopy (TEM) study (Hewat *et al.*, 2002) by displaying in great detail the main features described

Three supplementary figures and two tables are available with the online version of this paper.

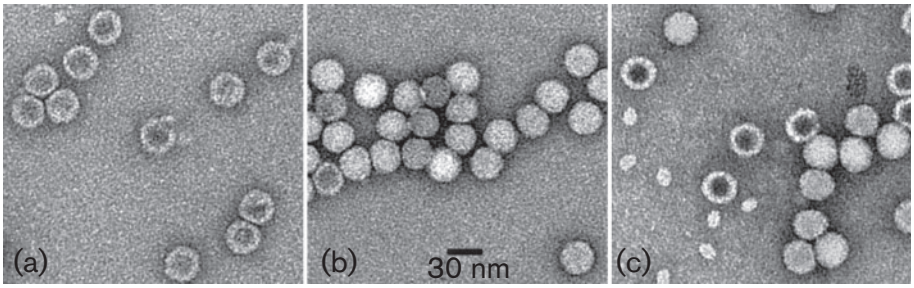

Fig. 1. Negatively stained electron micrographs of different TrV fractions collected during purification. Fractions were collected after 10–30 % sucrose gradient centrifugation and were dialysed overnight against NMT buffer (10 mM NaCl, 1 mM $MgCl_2$, 50 mM Tris/HCl pH 7.5). (a) Fraction collected at 22.5 % sucrose, composed of n-empty particles only. (b) Fraction collected at 30 % sucrose (bottom fraction), composed of virions (>90 %). (c) Fraction (b) after storage at 4 °C for 1 week. The preparation was composed of virions, n-empty particles and LSPs.

formerly for this virus. These characteristics are as follows: (i) their structures display a mean expansion of ~4 %, (ii) there is a reduction in the thickness of the protein shell, and (iii) there are structural rearrangements of the open channels of the proteins traversing the capsid. In this work, we have reported cryo-TEM reconstructions of full particles, natural EPs (n-empty), EPs produced experimentally by heating virions (e-empty) and EPs that appeared after storing virions for a few days (s-empty). A numerical analysis of the different cryo-TEM reconstructions enabled us to score the similarities between the different particles. Docking the atomic model of the TrV capsid proteins into the cryo-TEM reconstructions allowed us to estimate that no major changes had occurred to the capsid following genome release. Our observations indicated that RNA release in TrV produces an empty shell very similar to the mature virion capsid. In addition, LSPs resulting from the disassembly of the capsid were clearly associated with genome release. In contrast to similar studies, none of the three salient characteristics of the empty picornavirus models summarized above were observed in the TrV empty-capsid reconstructions.

RESULTS

Evolution of the population of TrV particles

TrV virions were separated from empty and other small particles (Fig. 1b) using the purification protocol described by Agirre *et al.* (2011). Following storage either at room (18 °C) or at a refrigerated (4 °C) temperature, a sample containing ~90 % virions (Fig. 1b) gave rise to a heterogeneous population containing both empty particles and LSPs (Fig. 1c). These LSPs could be concentrated with respect to the empty capsid and the virions. When this sample was visualized by TEM (Fig. 2a) using a negative-staining procedure, the LSPs showed a highly oriented distribution, offering almost a single view to the observer (Fig. 2a). SDS-PAGE analysis revealed that the LSPs were composed of the three main VPs (Fig. 2b). The two-dimensional averaging of these particles displayed two symmetrical domes that were related by a twofold axis with a size of ~13.5–15.0 nm long and 5.0–10.0 nm wide (Fig. 2c, 2d). Each of these two domes could be modelled by a pentamer of protomers or penton (5× VP1–3; Fig. 2d, right), which are found in each of the fivefold vertices in the TrV particle. Whilst LSPs can be obtained as a disassembly product from virions after storing them for a period of time, they were not observed as a by-product of e-empty particles. After incubation, we also observed a minor disassembly product in addition to the remaining full particles, EPs and LSPs. We were unable to characterize this population.

Cryo-TEM of full TrV particles

TrV virions frozen immediately after the last purification step appeared as smooth spheres of ~300 Å in diameter (Fig. 3). A three-dimensional (3D) reconstruction of these particles was obtained at 15.0 Å resolution (Figs 3 and 4). This reconstruction displayed a more detailed view of the features already observed in our previous negatively stained reconstruction obtained at 30 Å resolution (Estrozi *et al.*, 2008). The isosurface representation of TrV virions displayed five protuberances around the fivefold axes, contained a triangular plateau centred on the threefold axes (Fig. 3) and lacked the typical 'canyon' found in most picornaviruses (Rossmann *et al.*, 1987; Hewat *et al.*, 2000). In addition, we observed two features that were not recognizable in our former reconstruction, namely a hole traversing the capsid at the fivefold axes and a density at the capsid interior attributable to the RNA content (Fig. 3).

Cryo-TEM of TrV EPs

Three different EP reconstructions were obtained. The first, obtained at 19 Å resolution, corresponded to naturally occurring EPs purified directly from the insects (n-empty, Fig. 3) as described by Agirre *et al.* (2011). The second type of empty capsid, obtained by heating TrV virions (e-empty,

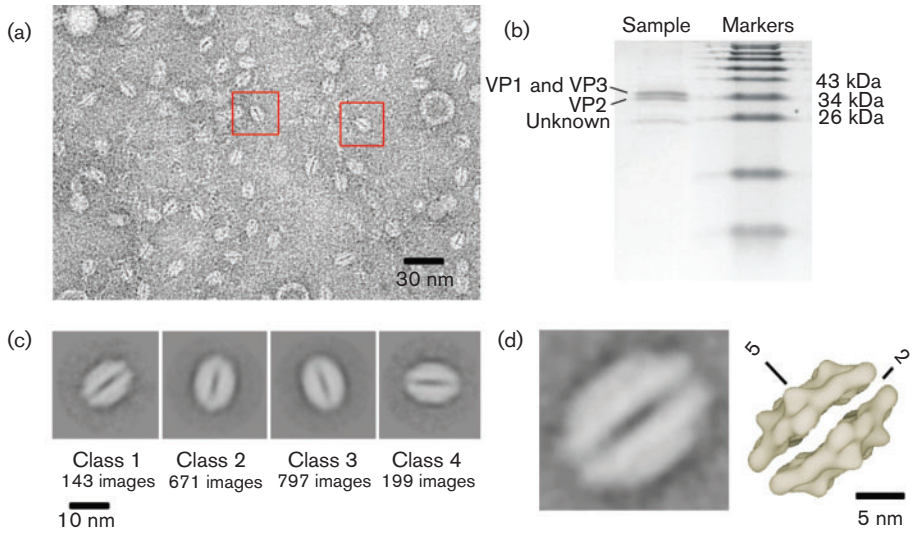

Fig. 2. Analysis of the LSPs. (a) Negatively stained electron micrograph of purified LSPs. (b) SDS-PAGE analysis of the LSPs observed in (a). A 15 μl sample from this preparation (concentration unknown) was run on a 15 % polyacrylamide gel. Two major bands were detected at ~34 kDa, corresponding to the expected molecular masses of the VPs of TrV. A third unidentified band was detected (at a lower intensity) below 26 kDa. (c) Four characteristic averaged images after hierarchical clustering with 143, 671, 797 and 199 particles. The two-dimensional averaging of the LSPs gave an image with two facing flattish lobes ~13.5–15 nm long and ~5–10 nm wide with an apparent twofold axis. (d) The left panel shows a close-up view of the first class shown in (c). The LSPs were composed of two symmetrical domes, each ~15 nm long and ~5 nm wide. The right panel shows a surface representation of an atomic model based on the TrV structure (Protein Data Bank 3NAP), filtered to 25 Å. The model was built by putting two pentons close to each other at an arbitrary distance of ~2 nm and facing according to the protein surface in contact with the RNA. Icosahedral fivefold and twofold axes are annotated '5' and '2', respectively.

Fig. 3) was reconstructed at 22 Å resolution. The third kind of empty particle (s-empty, Fig. 3), which appears following storage as described above, was reconstructed at 17 Å resolution. All three types of EP appeared as hollow spheres when observed under the microscope and were almost indistinguishable from each other (Fig. 3). The isosurface representations of the cryo-TEM reconstruction of n-empty particles displayed the same external features as those observed in virions (Fig. 3). The outer region of the e-empty reconstruction displayed predominantly identical features to those obtained for the s-empty particles (Fig. 3). The major difference between the n-empty and the two other types of EP reconstructions was a protruding extra density located at their twofold axes on the outer surface of both e- and s-empty particles (annotated as black ovals in Fig. 3). As in the n-empty particle, the full-particle isosurface did not show any outward density at the twofold symmetry points.

Quantitative particle comparison

The averaged densities from the three EP reconstructions showed that the thickness of the protein shells was ~34 Å (Fig. 5). This value coincided with the thickness of the TrV virion capsid reconstruction (Fig. 5, red line). To employ a global and quantitative criterion for pairwise comparison of the reconstructions, we computed two parameters: one was the correlation coefficient (CC), and the second was equivalent to the crystallographic *R*-factor (*R*). The similarity between each pair of the four reconstructions can be appreciated by comparing these values (Table S1, available in JGV Online). This analysis clearly showed that the virion reconstruction was most similar (high CC and low *R*) to the n-empty reconstruction (CC=0.93 and *R*=32.1). The comparison of the three types of EP reconstructions indicated that s-empty was more similar to e-empty (CC=0.96 and *R*=26.3) than to n-empty (CC=0.91 and *R*=35.6). These results were obtained considering the reconstructions as bulky objects and were consistent with the external appearance of the particles (Fig. 3).

Modelling the full and empty TrV capsids

To estimate the structural changes acting on the capsid proteins following genome release, we used the 'tectonic model' approach, which consists of fitting atomic models to the cryo-TEM reconstructions (Belnap *et al.*, 2000). The TrV protomer (VP1–3) was docked inside the reconstructed cryo-TEM map of the full capsid with a final CC of 0.74 and an *R* factor of 53.6 % (Fig. S1, panels b1 and c1). The root-mean-square deviation (RMSD) from the crystallographic position to the docked position was estimated to be 1.95 Å (Table S2). We then proceeded to

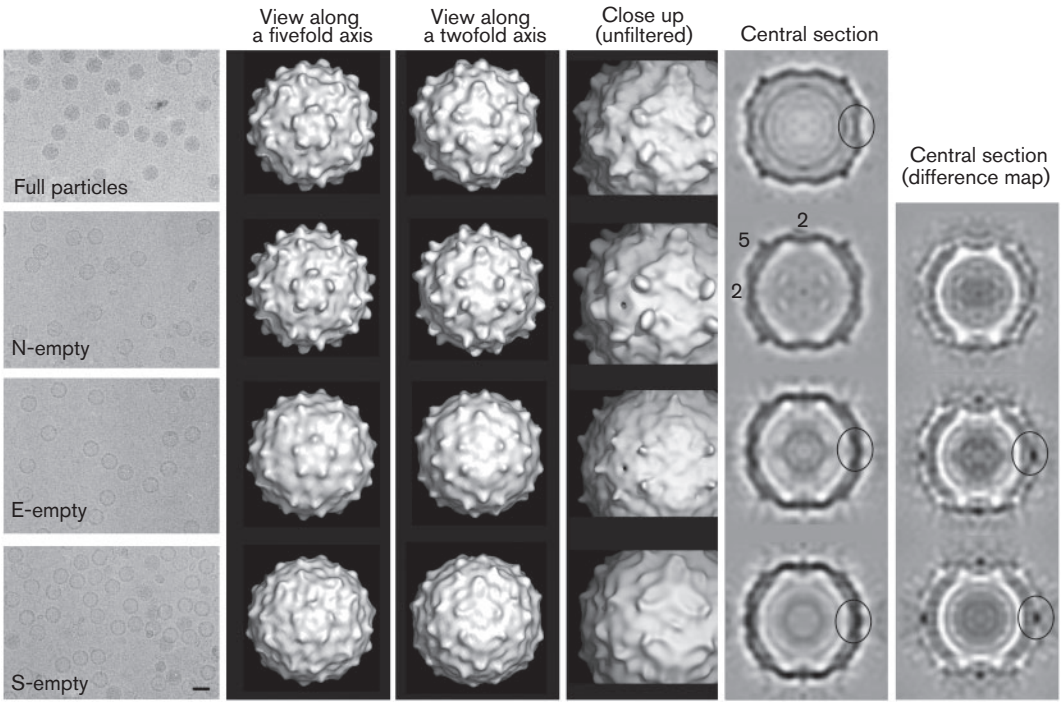

Fig. 3. Comparison of the four reconstructions. First column: electron micrographs of frozen hydrated TrV obtained from field-emission gun (full and s-empty) and Philips CM200 (n- and e-empty) microscopes operating at 200 kV. In the case of the s-empty particles, the micrograph shows a mixture of particles resulting from spontaneous RNA release and capsid disassembly. These different particles appeared in a sample that was originally composed of TrV virions, after 1 week of storage at 4 °C. In this micrograph, we can observe a major content of s-empty particles (some of them open), LSPs and a few unidentified small particles. Second and third columns: views along the five- and twofold axes of the four reconstructions, filtered to 22 Å, normalized and contoured at 1.1σ. Whilst the full and n-empty maps displayed a depression on the twofold axes, e- and s-empty particles showed a protuberance. Fourth column: close-up views along a twofold axis of the reconstructions (unfiltered), contoured at higher levels (full, 1.4σ; n-empty, 2.1σ; e-empty, 2.3σ; s-empty, 2.0σ). The protuberances of the e- and s-empty particles are clearly depicted. In the case of the e-empty particle, the hole in the fivefold axis is visible, whereas no other holes appeared in the surroundings. Fifth and sixth columns: central sections of the filtered and normalized reconstructions and of difference maps calculated by subtracting the density of each reconstruction from the density of the full particle (white, positive values; black, negative values). The black ovals indicate the density at the twofold axis.

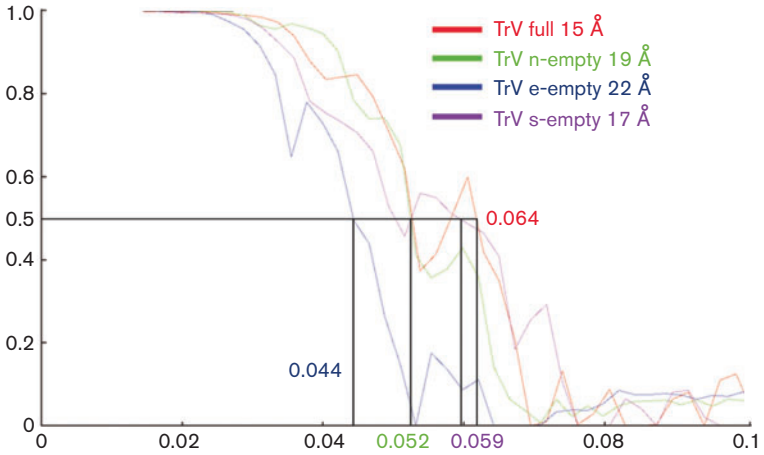

Fig. 4. Fourier shell correlation of the four reconstructions. Estimation of the resolutions by Fourier shell correlation of the full (red), n-empty (green), e-empty (blue) and s-empty (purple) 3D TrV reconstructions from half datasets. A correlation value of 0.5 was used.

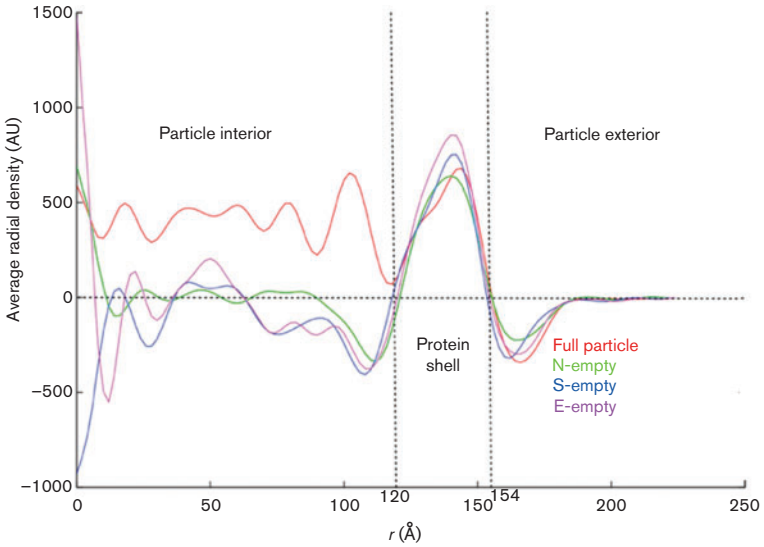

Fig. 5. Averaged density of the cryo-TEM reconstructions. The density from each of four reconstructions was averaged spherically and plotted as a function of the radius, *r* (Å). The horizontal dashed line indicates the density level corresponding to the external region (frozen solvent) and is a reference for zero density at the particle interior. The vertical dashed lines at values of 120 and 154 account for the estimated limits comprising the protein region, thus giving shell depths of ~34 Å.

make a best rigid body fit for each viral protein (Fig. S1, panels a2 and b2). The atomic models of each viral protein (in their crystallographic positions) were docked with a final CC of 0.75 and an *R* factor of 51.2 % (Fig. S1, panels c2 and d2). Calculating the RMSD values from the initial positions to the docked positions for each viral protein (Fig. 6), we obtained a mean value (2.43 Å) that was worse than that for the protomer (RMSD=3.7, 2.63 and 1.15 Å for VP1, -2 and -3, respectively; Table S2). For the n-empty particles, an identical fitting approach, as described above for the virions, was performed with the cryo-TEM map of the n-empty capsid. The atomic model was docked with a final CC of 0.87 and an *R* factor of 48.1 %. We then calculated the deviation between the crystallographic and the docked positions, and the RMSD value for the entire molecule was estimated to be 3.32 Å (Table S2). However, to visualize the eventual movements of the individual viral proteins, we performed a fit for each viral protein as described previously. We obtained a final CC of 0.89 and an *R* factor of 44.87 %. No major movements were detected for VP1 and VP3 (RMSD=2.41 and 3.26 Å, respectively; Table S2 and Fig. 6), whereas a slight movement of VP2 was observed (RMSD=6.55 Å; Table S2 and Fig. 6). We then proceeded in an analogous manner for the e-empty reconstruction. The atomic model was docked with a final CC of 0.81 and an *R* factor of 54.2 %. We then calculated the deviation between the crystallographic and the docked positions, and the RMSD value for the entire molecule was estimated to be 3.77 Å (Table S2). We again performed a fit for each viral protein, obtaining a final CC of 0.86 and an *R* factor of 48.9 %. Whereas no significant movement was detected for VP1 and VP3 (RMSD=2.94 and 3.12 Å, respectively; Table S2 and Fig. 6), an outward movement of VP2 was observed (RMSD=11.35 Å, Table S2 and Fig. 6). This movement mainly corresponded to a solid rotation and may account for the density redistribution around the capsid twofold axis (black oval in Fig. 3). This fitting is depicted in more detail in Fig. S2.

We did not apply the fitting calculations to the s-empty particles.

Stability of the TrV virions at neutral and low pH

Within the pH range 7.5–2.0, dynamic light scattering experiments indicated that the hydrodynamic diameter of TrV (full particles) remained essentially unaltered (Fig. 7, values indicated on the upper curve). In addition, within this pH range, the maximum fluorescence emission did not change appreciably (Fig. 7, middle and lower curves), indicating that none of the buried tryptophans became exposed to the solvent (the fluorescent emission of TrV virions denatured in 4 M guanidinium thiocyanate showed a maximum at 358 nm; Fig. 7). The increase in scattered light at pH values below 4 was the consequence of particle aggregation, an observation that was confirmed by electron microscopy imaging (data not shown). The large size of the aggregates at very acidic pH values prevented the measurement of particle size.

DISCUSSION

We have already referred to some studies on two picornaviruses comparing the structure of the infective virions with their empty particles. Whilst not intending to present a complete list of related works, other noteworthy studies on non-enveloped viruses include adeno-associated virus type 2 (Kronenberg *et al.*, 2005), foot-and-mouth-disease virus (Curry *et al.*, 1997), minute virus of mice (Agbandje-McKenna *et al.*, 1998), canine parvovirus (Wu & Rossmann, 1993), physalis mottle virus (Krishna *et al.*, 2001) and the plant viruses turnip yellow mosaic virus (van Roon *et al.*, 2004) and bean pod mottle virus (Lin *et al.*, 2003). Our results indicated that the TrV virions were stable from very acidic to neutral pH conditions, and this observation is consistent with the crystallographic studies

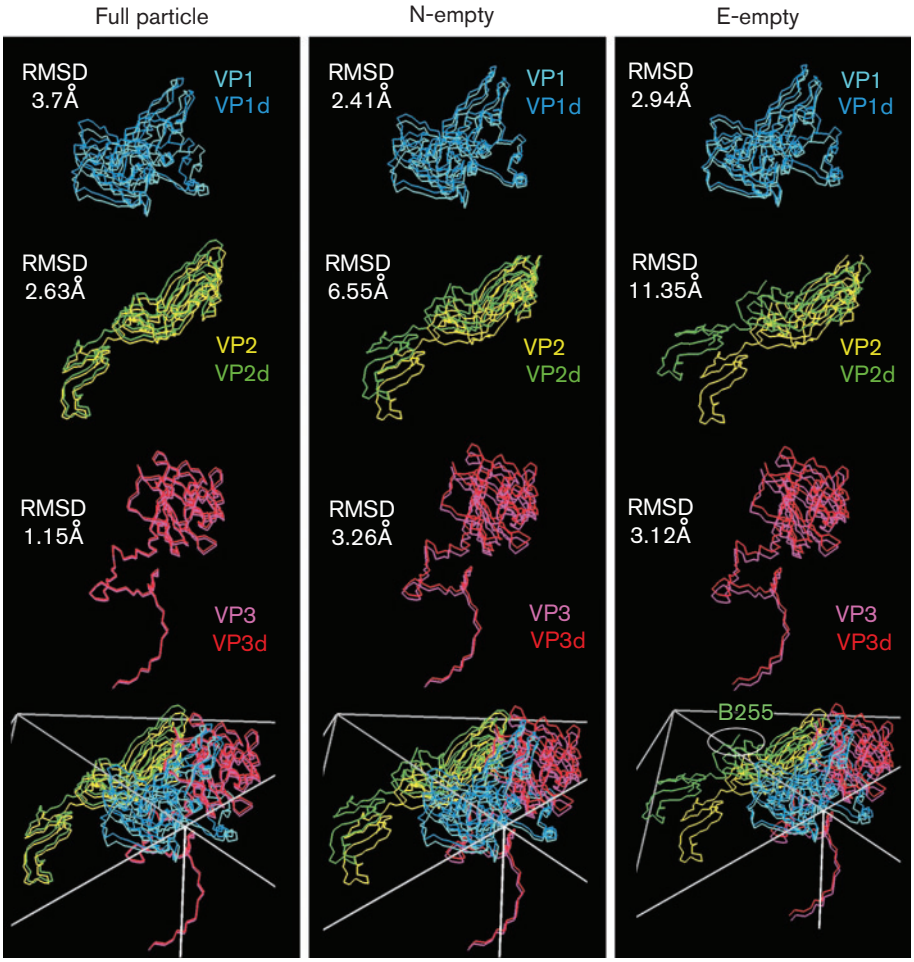

Fig. 6. Analysis of protein movements: superposition of the crystallographic and fitted positions (indicated by the suffix -d) in the cryo-TEM density maps of full, n- and e-empty particles. The lowest constructs show the assembled protomers with icosahedral symmetry support. In the case of the e-empty reconstruction, the C terminus of VP2 points clearly towards the twofold axis.

for which crystals obtained at pH 5.5 allowed the determination of the atomic structure of TrV (Rozas-Dennis *et al.*, 2004; Estrozi *et al.*, 2008). TrV infects the midgut of triatomines (Muscio *et al.*, 1987), and along the natural route of infection, this virus encounters a range of different pHs. The pH in the stomach of the insects can vary between 5.2 and 7.3, and in the small intestine, it ranges between 6.1 and 6.8 (Kollien *et al.*, 2001). Therefore, the acidic stability of TrV suggests that RNA release is not induced in the acidic pH-dependent manner that some picornaviruses employ. Our study comprised 3D cryo-TEM reconstruction of virions and n-empty particles of TrV at ~15 and ~19 Å resolution, respectively (Fig. 3). In contrast to our previous study (Estrozi *et al.*, 2008), we succeeded in selecting images from homogeneous samples using an effective purification procedure (Agirre *et al.*, 2011) and by obtaining the images directly after completing the purification, which avoided spontaneous *in vitro* disassembly. We also reported the *in vitro* spontaneous RNA release from TrV virions. Because the resulting particle products from this spontaneous disassembly contained a protein composition identical to that of the virions, we could exclude proteolysis as the cause of genome externalization and capsid disruption. We were then able to speculate that particle destabilization may occur as a consequence of a diffusion process and/or an imbalance of the forces that maintain the encapsulated genome.

Comparison between EPs

An important feature of all three EP reconstructions was that they accounted for a protein shell with equivalent thickness (Fig. 5). Due to the different protein composition of full and n-empty particles (Agirre *et al.*, 2011), n-empty particles probably never enclose the genome, thus representing a dead-end product of the assembly process. Therefore, only e-empty and s-empty structures are representative of the state of the capsid after RNA release. Reconstruction of the e-empty capsid allowed us to model

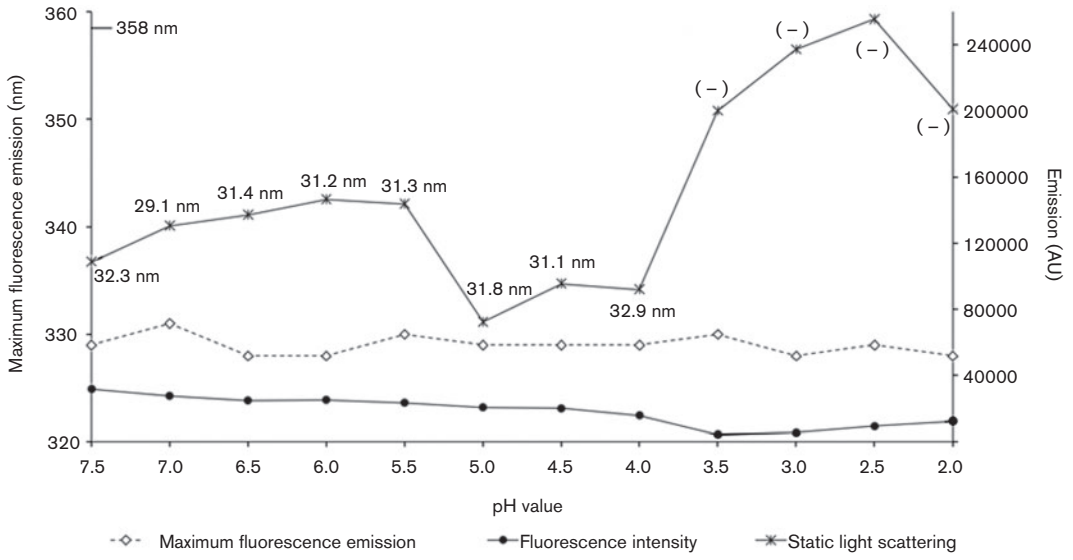

Fig. 7. Combined results from intrinsic fluorescence, static and dynamic light scattering. The absence of fluctuations in the maximum of the fluorescence emission (middle curve) indicates that there are no conformational changes in the environment of the tryptophan residues present in the TrV structure. The increase in the scattered light below pH 4 (top curve) is due to an aggregation process. There is also a slow but steady decrease in the fluorescence intensity (bottom curve), which may indicate that this aggregation process is continuous and incremental.

the structural changes that resulted in the TrV protein capsid following genome release. Although subtle, an interesting feature present in the reconstruction was the protuberance at the twofold axis particle surface (black ovals and negative peaks in the difference maps in Fig. 3). This extra density could be modelled with a solid movement of VP2 towards the capsid exterior (Fig. 6 and S2).

Comparison of full and e-empty capsids

The e-empty protein shell was successfully modelled using the 'tectonic model' approach (Fig. 6). The full and e-empty capsid reconstructions of TrV displayed one major difference, which was the density at the twofold axis already described. As this protuberance was also absent in the n-empty particles, it showed a trace of the genome externalization. Being at the frontier between two VP2 proteins right at the twofold axis, it may be assigned as the putative site for RNA egress. This hypothesis would be in agreement with recent studies on PV and HRV2 picornaviruses in which RNA externalization was shown to occur around the twofold axis (Bostina *et al.*, 2011; Garriga *et al.*, 2012). A second difference between the full and e-empty particle reconstructions was the narrowing of the hole located at the fivefold axis (Fig. 3). This narrowing could be attributed to slight rearrangements during the accommodation of the capsid proteins VP1 and VP3, which surround the fivefold axis. The mean densities of the reconstructions (Figs 5 and S3) showed that both particles had identical outer diameters. This identical size indicates that the capsid does not expand upon RNA release. This invariance of the protein shell contrasts with what has been described previously for HRV2 (Hewat *et al.*, 2002) and PV (Belnap *et al.*, 2000) EP reconstructions. In these two cases, capsid thinning was explained by the externalization of proteins located at the capsid interior that were previously in contact with the genome. This fact has been documented thoroughly for several members of the family *Picornaviridae* (Fricks & Hogle, 1990; Lewis *et al.*, 1998). With regard to the TrV e-empty capsids, such a process would not occur. Finally, aside from the subtle differences mentioned previously, the high similarity between the capsid of the full particles and that of the particles that released their RNA content indicated that, following genome release, no major rearrangements of the coat proteins occurred.

TrV capsid disassembly upon RNA release

LSPs of approximately 15 nm in length have been observed in previous TrV preparations (Estrozi *et al.*, 2008; Agirre *et al.*, 2011). So far, the origin of these small particles has been elusive. These particles were also obtained in the present study by storing a sample of TrV virions. The identification of their protein content after purification in a sucrose gradient (Fig. 2a) allowed us to confirm that these small particles are portions of the viral shell (Fig. 2b) and also that they constitute end products of capsid disassembly. A plausible explanation for the appearance of these particles is that they may be integrated by two facing pentons (Fig. 2d). It may seem unfavourable for TrV capsid assembly to

have pentons with a tendency to associate in dimers. A possible explanation to prevent this type of dimerization can be found in the role that VP4 may play in the processes of capsid building and dissociation. During assembly, VP4 is still part of the uncleaved VP0 precursor and would favour the interaction of the capsid intermediates (oligomers of protomers) with the genome, precluding the face-to-face dimerization of pentons. Upon capsid maturation, the excision of VP4 from VP0 occurs (Agirre *et al.*, 2011). The detachment of VP4 from the major capsid proteins upon genome release would enable the pentons to adopt the conformation of LSPs. As LSPs and isolated pentons are also observed in a fresh purification (Estrozi *et al.*, 2008), this indicates that both types of particle (i.e. pentons as capsid precursors and dimers of pentons as capsid disassembly products) co-exist *in vivo*. The structure and characteristics of these particles are subject to a more detailed study in a forthcoming article.

Conclusions

The experimental observations reported in this work show that RNA delivery in TrV produces empty capsids with features that differ from the characteristics observed in HRV2 (Hewat *et al.*, 2002; Garriga *et al.*, 2012) and PV (Belnap *et al.*, 2000). In Table 1, we have summarized the main features associated with RNA release in TrV and these two picornaviruses. The insect virus differs from the other viruses in that, upon genome release, the capsid does not change its outer diameter, whereas a 4 % global expansion is observed in both HRV2 and PV EPs. Moreover, in the two picornaviruses, the three major capsid proteins undergo substantial conformational changes that produce holes through which the genome can escape. Because there is no major protein movement after RNA delivery in TrV and pieces of the capsid appear as small particles upon genome release, we postulate a partial capsid cracking and/or dismantling mechanism associated with the RNA externalization process.

METHODS

Preparation and purification of TrV. Mature TrV and n-empty particles were purified from dry faeces fixed to paper fans of infected triatomines (colonies of *Triatoma infestans*), as described by Agirre *et al.* (2011).

Preparation of TrV EPs and LSP composition. E-empty particles were prepared as described by Hewat *et al.* (2002). A suspension of TrV virions was heated to 55 °C for 30 min immediately prior to the preparation of the cryo-TEM specimens. S-empty particles were obtained after the spontaneous RNA release that occurs when samples of TrV virions are stored under standard conditions (neutral pH, low ionic strength and temperatures of 4 and 18 °C). The evolution of full TrV particles over time was examined by negative-staining electron microscopy on a CM12 microscope (FEI) operating at 120 kV. Samples were stained with 1 % (w/v) ammonium molybdate and screened for the quality, concentration and nature of the viral particle population. Statistics were computed on several collected micrographs and performed over ~500 particles selected on different micrographs. For instance, for a typical sample containing 90±5 % virions and 10±5 % EPs, after 1 week of storage, the proportion became 70±5 % virions, 20±5 % EPs and 10±5 % LSPs, with a minor population of <5 % of very small non-identified particles. LSPs were isolated in a sucrose gradient, and their protein composition was analysed by SDS-PAGE.

Negative-stained image analysis and modelling of LSPs. LSPs were examined by negative-staining electron microscopy as described above. Micrographs were recorded and digitized on a Photoscan TD scanner (Z/I Imaging) at a step size of 14 μm. A total of 5800 particles were boxed from four different micrographs using the x3d program (Conway & Steven, 1999). Using the SPIDER software (Frank *et al.*, 1996), we performed classification by hierarchical clustering and obtained 17 classes by image averaging, with four significant ones. Classes showing side views represented 98 % of the particles on our images, preventing us from performing a 3D reconstruction.

Cryo-TEM images and image analysis. Specimens of interest were studied by cryo-TEM according to standard methods with a JEOL 2010F field-emission gun and on a CM200 microscope (FEI), both operating at 200 kV. Images were obtained under low electron dose conditions (<10 e/Å^2) and recorded at a nominal magnification of 40 000× at different defocus settings ranging from −1.2 to −4.0 μm. Micrographs were recorded on Kodak SO-163 film and developed for 12 min in full-strength Kodak D19. Negatives were screened by optical diffraction to reject drifted or astigmatic images, and selected images were digitized on a Photoscan TD scanner (Z/I Imaging) at a step size of 7 μm, corresponding to 1.75 Å per pixel at the sample. To perform the reconstruction, using the x3d program (Conway & Steven, 1999), approximately 5000, 2700, 2200 and 2800 particles were boxed from 25 and 15 (×3) different micrographs for full and n-, e- and s-empty TrV samples, respectively. Final reconstructions were obtained with the best 1716, 695, 573 and 1434 particles (after 30 refinement cycles) for full and n-, e- and s-empty TrV 3D maps, respectively. The TrV map obtained in a previous study (Estrozi *et al.*, 2008) was used as a starting model for the analyses. All subsequent refinements of particle origin and orientation were performed using the model-based polar Fourier transform programs (Baker & Cheng, 1996). The program CTFMIX (Conway & Steven, 1999) was used to correct the contrast transfer function effects and for the final Fourier–Bessel reconstruction. The resolutions were estimated by Fourier shell correlation of the reconstructions (Fig. 4) from half datasets using the criterion of 0.5 correlation (van Heel & Schatz, 2005). The isosurface representations of the reconstructed densities were rendered using RobEM (Fig. 3) and Amira (Mercury Computer Systems) (Fig. S3).

Comparison of cryo-TEM reconstructions. The cryo-TEM reconstructions were computed on orthogonal 3D grids with a spacing of 1.75 Å, and the corresponding average radial densities, each sampled at 2 Å, were computed by taking the mean value of the density within shells that were 5 Å wide. The limits of the protein shell were assigned to the points where the average radial density reaches the value corresponding to the exterior of the particle (frozen solvent). The distance between these two points represented a capsid thickness of ~34 Å, which was identical for all reconstructions. The correlation coefficients and crystallographic *R* factors used for the comparison between cryo-TEM particle reconstructions and the crystallographic TrV atomic model [Protein Data Bank (PDB) 3NAP] were calculated with the URO program (Navaza *et al.*, 2002) employing the Fourier coefficients within the 200–20 Å resolution range. For these calculations, the densities inside a sphere of radius 120 Å were set to zero in order to restrict the analysis to the region corresponding to the protein shell. All reconstructions were normalized, filtered to 22 Å resolution and subtracted for display in Fig. 3. Operations with maps were computed with MAPMAN (Kleywegt & Jones, 1996) and the CCP4 suite of programs (Winn *et al.*, 2011).

Table 1. Snapshots of RNA release in small non-enveloped icosahedral viruses

The current models of RNA release are based on the comparison of full (virions) and EPs of HRV2 (Hewat *et al.*, 2002; Garriga *et al.*, 2012), and empty and full (160S) PV particles (Lewis *et al.*, 1998; Levy *et al.*, 2010; Bostina *et al.*, 2011). This table summarizes the main characteristics associated with PV and HRV2 genome release together with the results reported here for TrV. EPs were prepared by heating purified virions as follows: TrV and HRV2, above 50 °C for 30 min, and PV at 50 °C for 3 min and 55 °C for 10 min for the 135S and 80S particles, respectively. LDR, low-density lipoprotein receptor; PVR, PV receptor; CDE, clathrin-dependent endocytosis; PFR, pocket factor release.

Virus	Capsid stability	Capsid modifications upon RNA release	RNA capsid exit	RNA translocation	Final structure
HRV2[1,2]	Unstable at pH <5.6[3,4] Breathing[5]	Low pH induces capsid expansion and PFR Substantial reorganization of the interpentamer interactions induces a capsid expansion and a shiftThe VP1 N terminus remains disordered in the capsid interior, whereas VP4 is extruded to the exterior with the RNA	Through an opening at the twofold axis (~10 Å wide and 30 Å long)	Through a membrane channel composed of VP4	Two types of 80S empty shells containing a variable amount of residual RNA[6]
PV[7,8,9]	Unstable upon cell attachment Stable at low pH[10] Breathing[11]	PVR attachment triggers the conversion of 160S into 135S particlesThe 135S intermediate externalizes the N terminus of VP1 and myrVP4RNA release produces 80S particles, which are slightly expanded with respect to the 160S particles VP1–3 proteins are shifted out of the capsid centre and rotated, resulting in significant alterations in the intersubunit contacts; these movements produce gaps approximately 30 Å wide between subunits The VP1 N-termini exit the capsid through pores that open at the base of the canyons	Through an opening at the base of the canyon and near a twofold axis	The insertion of myrVP4 and the N terminus of VP1 results in the formation of channels that facilitate the RNA translocation	Three types of 80S empty shells: 80S.e (partially filled with RNA), 80S.l and 'particles caught in the act' with RNA on both the inside and outside
TrV	Stable at pH 4.0–7.5 No breathing observed	Empty capsids have identical size and thickness to full RNA particles Capsid proteins VP1 and VP3 do not appreciably change their position upon RNA release The VP2 C terminus moves to the capsid exterior at the twofold axis. VP4 is disordered and exits the capsid with the RNA	Through a breach formed at the front of two symmetry-related protomers	Unknown (VP4 is disordered and is not myristoylated[12])	Empty capsids and small symmetrical particles (two facing pentons ~150 Å long and ~100 Å wide)

References: [1]Hewat *et al.* (2002); [2]Garriga *et al.* (2012); [3]Gruenberger *et al.* (1991); [4]Prchla *et al.* (1994); [5]Lewis *et al.* (1998); [6]Hewat & Blaas (2004); [7]Belnap *et al.* (2000); [8]Levy *et al.* (2010); [9]Bostina *et al.* (2011); [10]Pérez & Carrasco (1993); [11]Li *et al.* (1994); [12]PDB 3NAP; Agirre *et al.* (2011).

Fitting the TrV X-ray structures of VP1, -2 and -3 into the cryo-TEM reconstructed densities. To implement the 'tectonic model' (Belnap *et al.*, 2000), and as described in Results, the X-ray structures of the protomer VP1–3 and of each VP were positioned onto the cryo-electron microscope reconstructed densities using VEDA (http://mem.ibs.fr/VEDA). This software allowed the application of icosahedral symmetry to generate an entire capsid from the individually fitted protein structures, thus allowing us to discard significant clashes between neighbouring protomers. Several fitting parameters were set up, such as the resolution (100–20 Å for low- and high-resolution thresholds), the number of refinement cycles (one and three for the entire protomer VP1–3 and each individual VP, respectively) and the number of iterations.

Capsid stability under neutral and acidic pH conditions. To detect possible variations in the diameter of virions as a consequence of pH changes, we performed particle size measurements using dynamic light scattering. We also performed protein fluorescence spectroscopy and static light scattering. Due to the presence of seven tryptophans in each protomer, all isolated from the solvent, it was possible to detect the disassembly of the capsid proteins if the scattered light decreased or a shift in the maximum of fluorescence

emission was produced. Fluorescence spectra were obtained using a Jobin Yvon SPEX FluoroMax-3 fluorometer with an excitation wavelength of 295 nm and an emission range of 305–420 nm. Three independent measurements were interpolated using the GRAMS software. Static light scattering data were obtained with the same equipment but with excitation at 320 nm and collection of the scattering data in the range 315–325 nm. For each sample, the mean scattering intensity was calculated. Samples were prepared in 100 mM of the corresponding buffer (Tris for pH 7.0–7.5; citric acid for pH 2.0–6.5) and were incubated for 24 h before measurement. The concentration of TrV in each condition was 0.1 mg ml^{-1}, determined using a bicinchoninic acid assay (Pierce).

Image presentation. Figures were generated with VEDA (http://mem.ibs.fr/VEDA) and PyMOL (DeLano, 2002).

ACKNOWLEDGEMENTS

We thank Guy Schoehn and Elizabeth Hewat for their precious advice and comments. J. A. was awarded a short-term fellowship from EMBO (ASTF 309-2008) for a 3-month stay under the supervision of E. N. at the IBS, Grenoble. R. S.-E. acknowledges a pre-doctoral grant from the Basque Government (BG). G. A. M. is partially supported by ANPCyT (PICT no. 32618/05), Argentina. J. N. is grateful for an Ikerbasque fellowship to visit D. M. A. G.'s laboratory during 2011–2012. D. M. A. G. is grateful for the support of Bizkaia:Xede, UPV/EHU (IT-461-07), the BG (AE-2012-1-44 and MV-2012-1-41), CYTED (209RT0364) and MICINN (BFU2007-62062). D. M. A. G. is visiting professor at the Basque Country University (UPV/EHU).

REFERENCES

Agbandje-McKenna, M., Llamas-Saiz, A. L., Wang, F., Tattersall, P. & Rossmann, M. G. (1998). Functional implications of the structure of the murine parvovirus, minute virus of mice. *Structure* **6**, 1369–1381.

Agirre, J., Aloria, K., Arizmendi, J. M., Iloro, I., Elortza, F., Sánchez-Eugenia, R., Marti, G. A., Neumann, E., Rey, F. A. & Guérin, D. M. (2011). Capsid protein identification and analysis of mature *Triatoma* virus (TrV) virions and naturally occurring empty particles. *Virology* **409**, 91–101.

Baker, T. S. & Cheng, R. H. (1996). A model-based approach for determining orientations of biological macromolecules imaged by cryoelectron microscopy. *J Struct Biol* **116**, 120–130.

Belnap, D. M., Filman, D. J., Trus, B. L., Cheng, N., Booy, F. P., Conway, J. F., Curry, S., Hiremath, C. N., Tsang, S. K. & other authors (2000). Molecular tectonic model of virus structural transitions: the putative cell entry states of poliovirus. *J Virol* **74**, 1342–1354.

Bostina, M., Levy, H., Filman, D. J. & Hogle, J. M. (2011). Poliovirus RNA is released from the capsid near a twofold symmetry axis. *J Virol* **85**, 776–783.

Conway, J. F. & Steven, A. C. (1999). Methods for reconstructing density maps of "single" particles from cryoelectron micrographs to subnanometer resolution. *J Struct Biol* **128**, 106–118.

Curry, S., Fry, E., Blakemore, W., Abu-Ghazaleh, R., Jackson, T., King, A., Lea, S., Newman, J. & Stuart, D. (1997). Dissecting the roles of VP0 cleavage and RNA packaging in picornavirus capsid stabilization: the structure of empty capsids of foot-and-mouth disease virus. *J Virol* **71**, 9743–9752.

Czibener, C., La Torre, J. L., Muscio, O. A., Ugalde, R. A. & Scodeller, E. A. (2000). Nucleotide sequence analysis of *Triatoma* virus shows that it is a member of a novel group of insect RNA viruses. *J Gen Virol* **81**, 1149–1154.

DeLano, W. L. (2002). *The PyMOL User's Manual*. Palo Alto, CA: DeLano Scientific.

Estrozi, L. F., Neumann, E., Squires, G., Rozas-Dennis, G., Costabel, M., Rey, F. A., Guérin, D. M. A. & Navaza, J. (2008). Phasing of the *Triatoma* virus diffraction data using a cryo-electron microscopy reconstruction. *Virology* **375**, 85–93.

Frank, J., Radermacher, M., Penczek, P., Zhu, J., Li, Y., Ladjadj, M. & Leith, A. (1996). SPIDER and WEB: processing and visualization of images in 3D electron microscopy and related fields. *J Struct Biol* **116**, 190–199.

Fricks, C. E. & Hogle, J. M. (1990). Cell-induced conformational change in poliovirus: externalization of the amino terminus of VP1 is responsible for liposome binding. *J Virol* **64**, 1934–1945.

Garriga, D., Pickl-Herk, A., Luque, D., Wruss, J., Castón, J. R., Blaas, D. & Verdaguer, N. (2012). Insights into minor group rhinovirus uncoating: the X-ray structure of the HRV2 empty capsid. *PLoS Pathog* **8**, e1002473.

Gruenberger, M., Pevear, D., Diana, G. D., Kuechler, E. & Blaas, D. (1991). Stabilization of human rhinovirus serotype 2 against pH-induced conformational change by antiviral compounds. *J Gen Virol* **72**, 431–433.

Hewat, E. A. & Blaas, D. (2004). Cryoelectron microscopy analysis of the structural changes associated with human rhinovirus type 14 uncoating. *J Virol* **78**, 2935–2942.

Hewat, E. A., Neumann, E., Conway, J. F., Moser, R., Ronacher, B., Marlovits, T. C. & Blaas, D. (2000). The cellular receptor to human rhinovirus 2 binds around the 5-fold axis and not in the canyon: a structural view. *EMBO J* **19**, 6317–6325.

Hewat, E. A., Neumann, E. & Blaas, D. (2002). The concerted conformational changes during human rhinovirus 2 uncoating. *Mol Cell* **10**, 317–326.

Kleywegt, G. J. & Jones, T. A. (1996). xdlMAPMAN and xdlDATAMAN – programs for reformatting, analysis and manipulation of biomacromolecular electron-density maps and reflection data sets. *Acta Crystallogr D Biol Crystallogr* **52**, 826–828.

Kollien, A. H., Grospietsch, T., Kleffmann, T., Zerbst-Boroffka, I. & Schaub, G. A. (2001). Ionic composition of the rectal contents and excreta of the reduviid bug *Triatoma infestans*. *J Insect Physiol* **47**, 739–747.

Krishna, S. S., Sastri, M., Savithri, H. S. & Murthy, M. R. (2001). Structural studies on the empty capsids of physalis mottle virus. *J Mol Biol* **307**, 1035–1047.

Kronenberg, S., Böttcher, B., von der Lieth, C. W., Bleker, S. & Kleinschmidt, J. A. (2005). A conformational change in the adeno-associated virus type 2 capsid leads to the exposure of hidden VP1 N termini. *J Virol* **79**, 5296–5303.

Levy, H. C., Bostina, M., Filman, D. J. & Hogle, J. M. (2010). Catching a virus in the act of RNA release: a novel poliovirus uncoating intermediate characterized by cryo-electron microscopy. *J Virol* **84**, 4426–4441.

Lewis, J. K., Bothner, B., Smith, T. J. & Siuzdak, G. (1998). Antiviral agent blocks breathing of the common cold virus. *Proc Natl Acad Sci U S A* **95**, 6774–6778.

Li, Q., Yafal, A. G., Lee, Y. M., Hogle, J. & Chow, M. (1994). Poliovirus neutralization by antibodies to internal epitopes of VP4 and VP1 results from reversible exposure of these sequences at physiological temperature. *J Virol* **68**, 3965–3970.

Lin, T., Cavarelli, J. & Johnson, J. E. (2003). Evidence for assembly-dependent folding of protein and RNA in an icosahedral virus. *Virology* **314**, 26–33.

Mayo, M. A. (2002). Virus taxonomy – Houston 2002. *Arch Virol* **147**, 1071–1076.

Muscio, O. A., LaTorre, J. L. & Scodeller, E. A. (1987). Small nonoccluded viruses from triatomine bug *Triatoma infestans* (Hemiptera: Reduviidae). *J Invertebr Pathol* **49**, 218–220.

Muscio, O. A., La Torre, J. L. & Scodeller, E. A. (1988). Characterization of *Triatoma* virus, a picorna-like virus isolated from the triatomine bug *Triatoma infestans*. *J Gen Virol* **69**, 2929–2934.

Navaza, J., Lepault, J., Rey, F. A., Alvarez-Rúa, C. & Borge, J. (2002). On the fitting of model electron densities into EM reconstructions: a reciprocal-space formulation. *Acta Crystallogr D Biol Crystallogr* **58**, 1820–1825.

Pan American Health Organization (1993). *Estimación cuantitativa de la enfermedad de Chagas en las Américas*. Montevideo, Uruguay: Organización Panamericana de la Salud. http://www.bvsops.org.uy/pdf/chagas19.pdf.

Pérez, L. & Carrasco, L. (1993). Entry of poliovirus into cells does not require a low-pH step. *J Virol* **67**, 4543–4748.

Prchla, E., Kuechler, E., Blaas, D. & Fuchs, R. (1994). Uncoating of human rhinovirus serotype 2 from late endosomes. *J Virol* **68**, 3713–3723.

Rossmann, M. G., Arnold, E., Erickson, J. W., Frankenberger, E. A., Griffith, J. P., Heck, H. J., Johnson, J. E., Kramer, G., Luo, M. & other authors (1987). The structure of a human common cold virus (rhinovirus 14) and its functional relations to other Picornaviruses. In *Crystallography in Molecular Biology*, pp. 263–280. Edited by D. Moras, J. Drenth, B. Strandberg, D. Suck & K. Wilson. New York & London: Plenum Press.

Rozas-Dennis, G. S., Squires, G., Pous, J., Costabel, M. D., Lepault, J., Navaza, J., Rey, F. A. & Guérin, D. M. (2004). Purification, crystallization and preliminary X-ray analysis of *Triatoma* virus (TrV) from *Triatoma infestans*. *Acta Crystallogr D Biol Crystallogr* **60**, 1647–1650.

van Heel, M. & Schatz, M. (2005). Fourier shell correlation threshold criteria. *J Struct Biol* **151**, 250–262.

van Roon, A. M., Bink, H. H., Plaisier, J. R., Pleij, C. W., Abrahams, J. P. & Pannu, N. S. (2004). Crystal structure of an empty capsid of turnip yellow mosaic virus. *J Mol Biol* **341**, 1205–1214.

Winn, M. D., Ballard, C. C., Cowtan, K. D., Dodson, E. J., Emsley, P., Evans, P. R., Keegan, R. M., Krissinel, E. B., Leslie, A. G. & other authors (2011). Overview of the CCP4 suite and current developments. *Acta Crystallogr D Biol Crystallogr* **67**, 235–242.

Wu, H. & Rossmann, M. G. (1993). The canine parvovirus empty capsid structure. *J Mol Biol* **233**, 231–244.